Pergamon

Tetrahedron 57 (2001) 2769–2774

TETRAHEDRON

Theoretical study of hydrogenolysis termination processes in ethylene polymerization

L. Petitjean,[a] D. Pattou[a,†] and M. F. Ruiz-López[b,*]

[a]*Groupement de Recherches de Lacq, ATOFINA, BP 34, 64170 Artix, France*
[b]*Laboratoire de Chimie Théorique, UMR CNRS-UHP 7565 (part of the Institut Nancéien de Chimie Moléculaire), Université Henri Poincaré Nancy I, BP 239, 54506 Vandoeuvre-les-Nancy Cedex, France.*

Received 23 May 2000; revised 22 January 2001; accepted 31 January 2001

Abstract—The reaction of molecular hydrogen with the active species of a model metallocene catalyst is investigated through quantum mechanical calculations. The results are compared to ethylene insertion in the corresponding polymerization reaction. Hydrogenolysis and ethylene insertion exhibit both *frontside* and *backside* mechanisms. However, while ethylene insertion proceeds preferably through frontside mechanism, hydrogenolysis occurs mainly through the backside one. The activation energies are close but hydrogenolysis is slightly more favorable than ethylene insertion, in agreement with experimental findings. Agostic interactions have been found to play an important role, like in the chain propagation process. © 2001 Elsevier Science Ltd. All rights reserved.

1. Introduction

The most important industrial application of organometallic chemistry is the Ziegler–Natta catalysis of olefin polymerization. It involves a heterogeneous catalyst such as $TiCl_4$ supported on an $MgCl_2$ matrix. The length of the polymer chains obtained depends on the competition between chain propagation and chain termination reactions. In most cases, propagation is much easier than termination so that, in industrial production, the chain growth is regulated by injection of molecular hydrogen into the reactor. The sensitivity of heterogeneous catalysts to H_2 is highly variable and is not completely understood. Therefore, a better knowledge of the hydrogenation process would be useful to control efficiently the chain growth of the polymer as well as its physical properties (molecular masses, melt index, crystallinity…). Unfortunately, the molecular modeling of such industrial reactions is a very hard task for different reasons, particularly because the structure of the active species is unknown.

Nevertheless, it is generally accepted in the literature that heterogeneous and homogeneous polymerization mechanisms are very close. Homogeneous catalysis with metallocenes has seen an important development since the discovery of their activation by MAO[1,2] and much theoretical work has been devoted to it.[3–23] One may then be inclined to extrapolate the conclusions reached in the study of hydrogenolysis in metallocene catalysis to the case of heterogeneous catalysis. Moreover, hydrogenolysis processes in metallocene catalysis are of substantial interest for industrial companies since, in practice, injection of H_2 stops the polymerization, which renders the control of the chain growth difficult.

In a previous work,[24] we have reported a theoretical analysis of the reaction mechanism for ethylene polymerization in the presence of a model metallocene catalyst. Here, we focus on the reaction of such a system with molecular hydrogen. Our aim is to compare both processes in order to get a deeper insight on the factors determining the competition between propagation (reaction with ethylene) and termination (reaction with H_2). To the best of our knowledge, the hydrogenolysis process has not been theoretically investigated, though related reactions has received some attention.[25–28]

2. Computational details—model description

The calculations have been carried out using the Density Functional Theory (DFT) approach and the GAUSSIAN 94 package.[29] The basis set D95[30] has been employed for C and H atoms. For Zr a double-ζ basis set together with Los Alamos effective core potentials for the description of core electrons have been used.[30] All calculations have been done with the BLYP exchange-correlation functional.[30]

The geometries have been fully optimized without any constraints or symmetry conditions. Transitions structures (TSs) have been located using a quasi-Newton approach.[31]

Keywords: polymerization; catalysis; theoretical Studies; hydrogenolysis.
* Corresponding author. Tel.: +33-383-912050; fax: +33-383-912530; e-mail: manuel.ruiz@lctn.uhp-nancy.fr
† Fax: +33-559-926765; e-mail: denis.pattou@atofina.fr

PII: S0040-4020(01)00132-6

Scheme 1.

Free energy values have been computed in some cases using standard methods.

As in previous works, the active species is assumed to be the cation $[Cp_2ZrEt]^+$, where Cp represents a cyclopentadienyl ring (see Scheme 1). For such a species, several agostic bonds may be imagined. These bonds result from the interaction of an H-atom in the chain with the metal. In principle, depending on the position of the H-atom, α-H, β-H, γ-H or δ-H agostic are possible (see Scheme 2). Nevertheless, it has been already shown that the β-H agostic interaction is the most favorable one in the resting state.[32] The structure of the predicted β-H active species is shown in Fig. 1.

Like in the case of the propagation reaction, the attack in the hydrogenolysis step may proceed in two ways depending on the relative position of the H_2 molecule with respect to the β-agostic hydrogen. Thus, *syn* or *anti* processes must be considered that lead to reaction mechanisms known as *frontside* and *backside*. They are schematically explained in Scheme 3 and will be described in detail below. For clarity, we present the structures in the Figs. 1–4 with one apparent Cp ring only.

3. Results

3.1. Frontside mechanism

The structures corresponding to this mechanism are drawn in Fig. 2. As already explained, the reaction begins with the formation of a β-H *syn* complex **I** in which H_2 adopts a perpendicular orientation with respect to the middle plane of the molecule. In complex **I**, the hydrogen molecule is not in a favorable position to react with the carbon atom linked to the metal (C_α). Thus, the process proceeds in two steps: (a) chain rotation through transition structure **II** to yield the α-H agostic complex **III** and (b) hydrogenolysis through TS **IV** to yield **V**. In other words, the reaction path parallels that predicted for the frontside insertion of the ethylene molecule in the polymerization reaction.

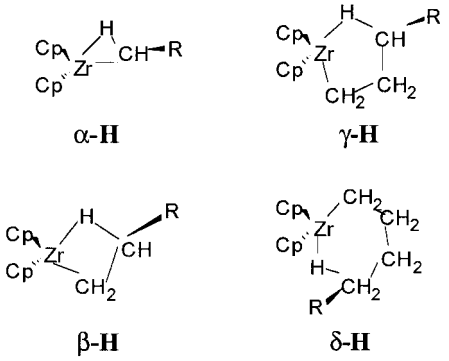

Scheme 2.

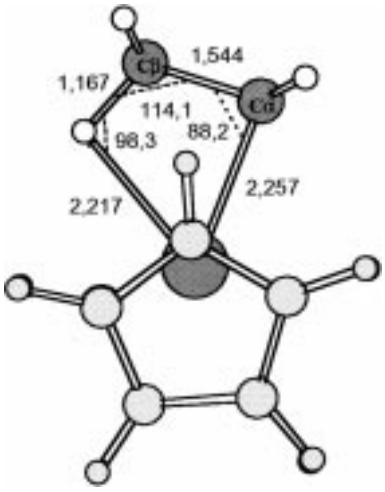

Figure 1. Computed structure for the active species resting state.

Complexation does not affect much the structure of the β-H active species, as shown by comparison of structure **I** with the resting state in Fig. 1. Note, however, that the Zr–C, Zr–H and H–H bond lengths are slightly increased although the changes are small compared to those predicted for the complexation of the same active species with ethylene.[24] This is the expected result on the basis of the higher electron donation power of ethylene.

In transition structure **II**, the chain rotates and an α-H bond is partially formed. Complex **III** is an α-H species in which H_2 lies in the middle plane of the molecule[24] with shorter

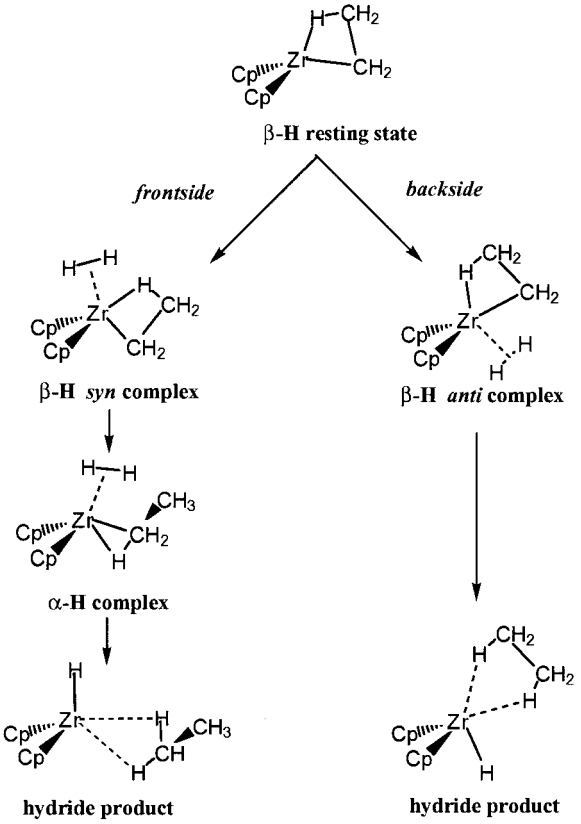

Scheme 3.

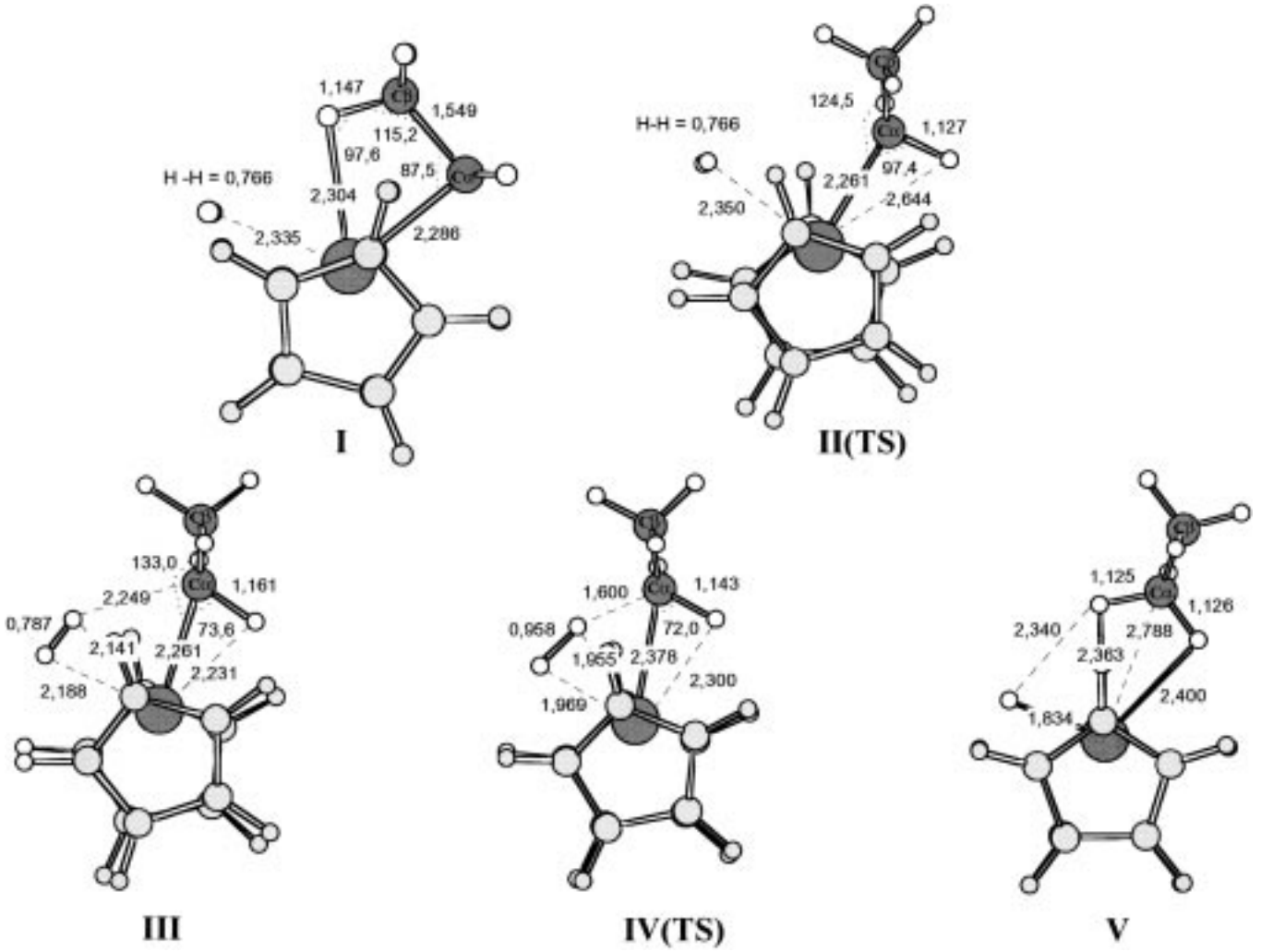

Figure 2. Structures involved in the frontside mechanism, which involves complexation (**I**) chain rotation (TS **II**, intermediate **III**) and hydrogenolysis (TS **IV**, product **V**).

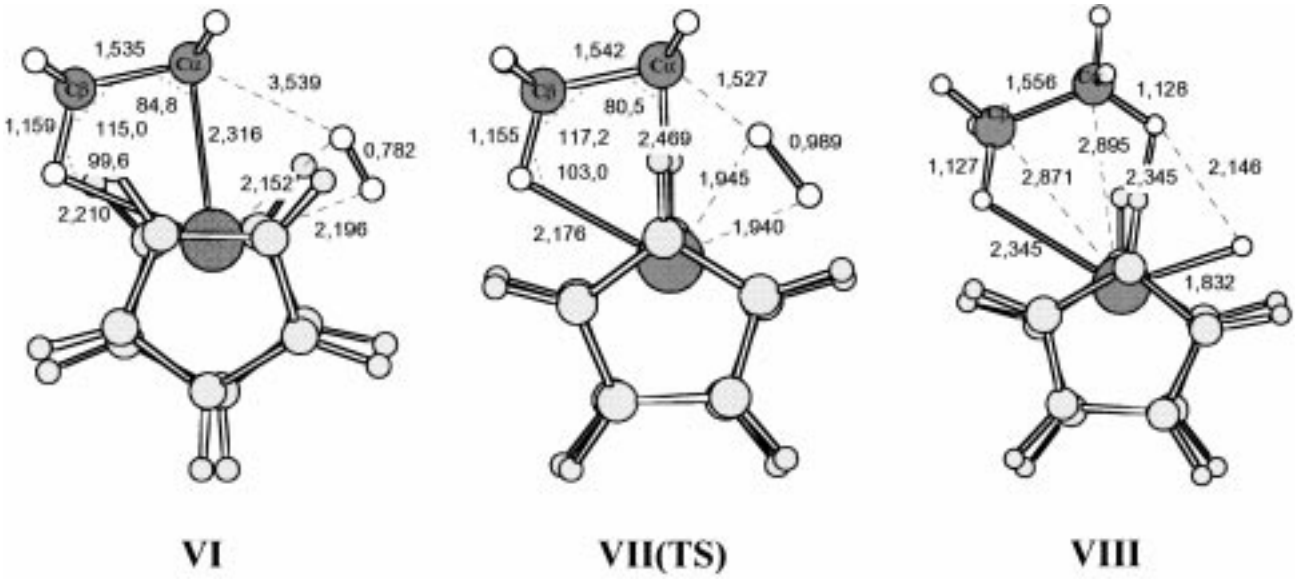

Figure 3. Structures involved in the backside mechanism, which involves complexation (**VI**) and direct insertion (TS **VII**, product **VIII**).

metal–H_2 distance. The H–H bond is elongated by 0.02 Å. Note that the metal–H_2 coordination becomes asymmetric. As a consequence, the hydrogen atom situated closer to the metal may now react with the carbon atom. Note also that the α-H bond is 0.04 Å shorter than the one observed in the corresponding ethylene complex.[24]

The transition structure **IV** of the insertion step is similar to structure **III**. The main features are the lengthening of the H–H distance (by 0.18 Å), the shortening of the H–C_α distance (by 0.65 Å) and the shortening of the H_2 molecule–Zr distance (by 0.2 Å). Another remarkable result is that the α-H bond is weakened in this transition structure. Finally, in product **V**, the formed ethane molecule is still linked to the metal through hydrogen atoms. The length of the formed Zr–H bond is comparable to those found in hydrides.

3.2. Backside mechanism

In the starting complex, the carbon linked to the metal is already accessible for reaction with hydrogen so that backside hydrogenolysis proceeds in a one step process. Structures obtained for the initial complex **VI**, the transition state **VII** and the final product **VIII** are drawn in Fig. 3. The reaction is close to the backside ethylene insertion described in previous work.[24]

In complex **VI**, the H_2 molecule lies in the middle plane of the catalyst. The Zr–H and the H–H distances are comparable to those observed for complex **III**. The Zr–C_α–C_β–H_{ag} plane is not modified by H_2 complexation. Structure **VI** is comparable to that found for the ethylene-resting state complex in our previous work.[24] In TS **VII**, one notes the expected trends for the reaction coordinate: H–H elongation (0.2 Å), Zr–H_2 shortening (0.2 Å) and C_α–H shortening (1.01 Å). A striking feature is the contraction of the agostic bond (0.03 Å), which demonstrates the importance of the role this type of bond plays in the process. One can also remark that the H_2 molecule does not move out of the middle plane of the system. The product **VIII** displays

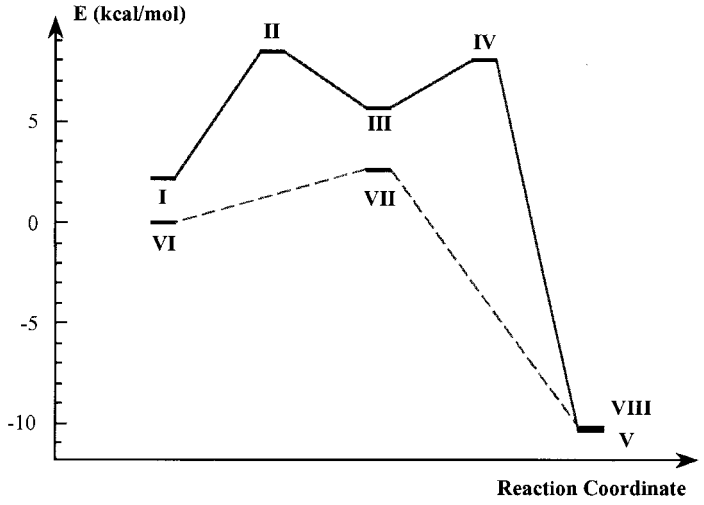

Figure 4. Comparison of frontside (single line) and backside (dashed line) hydrogenolysis energetics.

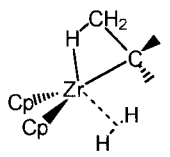

H_2 β-H *anti* complex

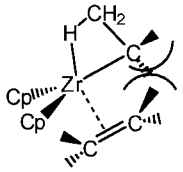

ethylene β-H *anti* complex

Scheme 4.

two metal–H agostic bonds, like **V**, although now the hydrogen atoms belong to different carbon atoms. The corresponding distances in **VIII** are shorter than that in **V**. Finally, the non-agostic metal–H bond is strong, its length being comparable to that predicted in **V**.

3.3. Energetics

The energy profiles for the two hydrogenolysis mechanisms are given in Fig. 4. The first step in the frontside path is endothermic (3.5 kcal/mol) with an activation energy of 6.4 kcal/mol. Conversely, the second step is quite exothermic (16.1 kcal/mol) with smaller activation barrier, 2.4 kcal/mol. The starting complex of the backside reaction is more stable than the corresponding frontside one by 2.2 kcal/mol. Moreover, the backside mechanism is exothermic (10.2 kcal/mol) and displays a small barrier of 2.8 kcal/mol. Although the differences between the different activation energies are not quite large, our computations suggest that the backside reaction path could be slightly more favorable than the frontside one. This result is in contrast with the conclusions reached for ethylene insertion, for which the frontside mechanism is preferred.[24] The origin of this difference could be related to steric hindrance factors. Indeed, the hydrogen molecule can approach the growing chain in the *anti* orientation easily, which is suitable for the reaction to proceed. Conversely, the ethylene molecule interacts strongly with the chain in the *anti* approach and the *syn* conformation appears to be more favorable. (see Scheme 4)

If one compares the activation barriers for hydrogenolysis and insertion (2.8 and 3.1 kcal/mol,[24] respectively) the former reaction is predicted to be a little bit more favorable, although the energy difference is below the computational accuracy. On the other hand, complexation of the active species with H_2 is less exothermic than complexation with ethylene (−5.3 and −6.6 kcal/mol,[24] respectively).

Thermodynamic computations have been carried out in order to compare the free energies of activation for the hydrogenolysis and insertion processes. Our results predict:

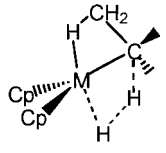

tetrahedral complex

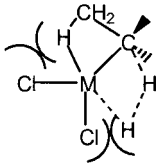

octahedral complex

Scheme 5.

$\Delta G_{hydrogenolysis}$=2.7 kcal/mol and $\Delta G_{insertion}$=4.6 kcal/mol. The latter value is an estimation that we have made using structures **III** and **XI** of Ref. 24 for which we have carried out the calculation of the frequencies of vibration. Structure **III** has been assumed to be the reactive species in the frontside insertion mechanism[19] although in our previous work[24] we have shown that another (less stable) complex could play such a role. Structure **XI** is the highest TS in frontside ethylene polymerization. We recall that such a reaction proceeds through a stepwise mechanism. The rate-limiting step is the last one, which corresponds to insertion (structures **VIII** and **XI** in Ref. 24). Further calculations have shown that the free energy of activation for this insertion step is 3.4 kcal/mol. Therefore, all these thermodynamic data confirms the preference for hydrogenolysis with respect to ethylene insertion. Our results are consistent with experimental studies that describe H_2 as an efficient transfer agent in polymerization processes with metallocene catalysts.

On the basis of the above results, it is interesting to look at the factors that can decrease the affinity of the metallocene catalyst for molecular hydrogen. In fact, if one is able to control this affinity, the chain growth might be regulated modulating the hydrogen pressure in the reactor. This goal could possibly be achieved by increasing the steric hindrance in the middle plane of the molecule. In such conditions, the backside hydrogenolysis mechanism should be disfavored because the formation of the transition state, in which five atoms are coplanar (the H_2 molecule and the C_α, C_β, H_β atoms), would require a larger activation energy. Then, hydrogenolysis and ethylene insertion would both proceed through the frontside mechanism and the latter reaction would be the preferred one.

The same reasoning can also explain why H_2 is less efficient in heterogeneous catalysis. Though such a hypothesis would require confirmation by further computations, one can do a qualitative analysis based on symmetry considerations. Whereas in the case of a metallocene, the Zr atom lies in a pseudo-tetrahedral environment, in heterogeneous systems, the Ti atom lies in an octahedral environment. As shown in Scheme 5, one may expect larger steric hindrances in the middle plane of the molecule for the octahedral arrangement, disfavoring the backside hydrogenolysis mechanism.

4. Conclusions

Hydrogenolysis proceeds through a backside mechanism, in contrast with ethylene insertion. Both processes involve small activation energies, the computed hydrogenolysis barrier being 0.3 kcal/mol lower than the insertion one. Though this value is probably below the accuracy of the theoretical model, the main conclusions of the present work is that the observed preference for hydrogenolysis with respect to ethylene insertion may be related to the stereochemistry of the reactions.

A possible way to control the kinetics of the hydrogenolysis reaction has been proposed. It consists on the increase of steric hindrance in the middle plane of the system in order to impede backside hydrogenolysis. A similar reasoning leads

to the hypothesis that differences on H_2 sensibility between heterogeneous and homogeneous catalysis could be related to local symmetry around the metal center. Thus, the present results could be useful in the design of new homogenous catalysts with reduced hydrogen affinity.

Acknowledgements

We thank ATOFINA Corp. for authorization to publish this work. We are also grateful to Dr Saudemont and Dr Malinge from Groupement de Recherches de Lacq (ATOFINA) for their collaboration in this project. Finally, we acknowledge the referee for useful comments on the manuscript.

References

1. Sinn, H.; Kaminsky, W.; Vollmer, H. J.; Woldt, R. *Angew. Chem.* **1980**, *18*, 99.
2. For review on metallocene catalysts see: Brintzinger, H. H.; Fischer, D.; Müllhaupt, R.; Rieger, B.; Waymouth, R. M. *Angew. Chem., Int. Ed. Engl.* **1995**, *34*, 1143.
3. Siegbahn, P. E. M.; Strömberg, S.; Zetterberg, K. *Organometallics* **1996**, *15*, 5542–5550.
4. Bierwagen, E. P.; Bercaw, J. E.; Goddard III, W. A. *J. Am. Chem. Soc.* **1994**, *116*, 1481–1489.
5. Weiss, H.; Ehrig, M.; Ahlrichs, R. *J. Am. Chem. Soc.* **1994**, *116*, 4919.
6. van Dormemaele, G. H. J.; Meier, R. J.; Iarlori, S.; Buda, F. *Theochem* **1996**, *363*, 269.
7. Fusco, R.; Longo, L. *Macromol. Symp.* **1995**, *89*, 197–202.
8. Cavallo, L.; Guerra, G. *Macromolecules* **1996**, *29*, 2729.
9. Koga, N.; Yoshida, T.; Morokuma, K. In *Ziegler Catal.*; Furk, G., Mülhaupt, R., Brintzinger, H. H., Eds.; Springer: Berlin, 1995; pp 277–289.
10. Yoshida, T.; Koga, N.; Morokuma, K. *Organometallics* **1995**, *14*, 746.
11. Yoshida, T.; Koga, N.; Morokuma, K. *Organometallics* **1996**, *15*, 766–777.
12. Koga, N.; Yoshida, T.; Morokuma, K. *Polym. Mater. Sci. Engng* **1996**, *74*, 360–361.
13. Woo, T. K.; Fan, L.; Ziegler, T. *Organometallics* **1994**, *13*, 432–433.
14. Woo, T. K.; Fan, L.; Ziegler, T. *Organometallics* **1994**, *13*, 2252.
15. Fan, L.; Harrison, D.; Deng, L.; Woo, T. K.; Swerhone, D.; Ziegler, T. *Can. J. Chem.* **1995**, *73*, 989.
16. Fan, L.; Harrison, D.; Deng, L.; Woo, T. K.; Ziegler, T. *Organometallics* **1995**, *14*, 2018.
17. Woo, T. K.; Fan, L. In *Ziegler Catal.*; Furk, G., Mülhaupt, R., Brintzinger, H. H., Eds.; Springer: Berlin, 1995; pp 293–315.
18. Lohrenz, J. C.; Woo, T. K.; Fan, L.; Ziegler, T. *J. Organomet. Chem.* **1995**, *497*, 91.
19. Lohrenz, J. C.; Woo, T. K.; Ziegler, T. *J. Am. Chem. Soc.* **1995**, 12973.
20. Margl, P.; Ziegler, T. *J. Am. Chem. Soc.* **1996**, *118*, 7337–7344.
21. Margl, P.; Ziegler, T. *Organometallics* **1996**, *15*, 5519–5523.
22. Woo, T. K.; Margl, P. M.; Lohrenz, J. C. W.; Böchl, P. E.; Ziegler, T. *J. Am. Chem. Soc.* **1996**, *118*, 13021–13030.
23. Margl, P.; Lohrenz, J. C. W.; Ziegler, T.; Blöchl, P. E. *J. Am. Chem. Soc.* **1996**, *118*, 4434–4441.
24. Petitjean, L.; Pattou, D.; Ruiz-Lopez, M. F. *J. Phys. Chem. B* **1999**, *103*, 27.
25. Dedieu, A. *Chem. Rev.* **2000**, *100*, 543.
26. Ziegler, T.; Folga, E.; Berces, A. *J. Am. Chem. Soc.* **1993**, *115*, 1305.
27. Musaev, D. G.; Froese, R. D. J.; Morokuma, K. *New J. Chem.* **1997**, *21*, 1269.
28. Torrent, M.; Solà, M.; Frenking, G. *Chem. Rev.* **2000**, *100*, 439.
29. Frisch, M. J.; Trucks, G. W.; Schlegel, H. B.; Gill, P. M. W.; Johnson, B. G.; Robb, M. A.; Cheeseman, J. R.; Keith, T.; Petersson, G. A.; Montgomery, J. A.; Raghavachari, K.; Al-Laham, M. A.; Zakrzewski, V. G.; Ortiz, J. V.; Foresman, J. B.; Peng, C. Y.; Ayala, P. Y.; Chen, W.; Wong, M. W.; Andres, J. L.; Replogle, E. S.; Gomperts, R.; Martin, R. L.; Fox, D. J.; Binkley, J. S.; Defrees, D. J.; Baker, J.; Stewart, J. P.; Head-Gordon, M.; Gonzalez, C.; Pople, J. A. GAUSSIAN 94, Revision D.3; Gaussian: Pittsburgh PA, 1995.
30. For the D95 basis set, see: Dunning, Jr., T. H.; Hay, P. J. In *Modern Theoretical Chemistry*; Schaeffer III, H. F., Ed.; Plenum: New-York, 1976; pp 1–128. For Zr basis set, see: Hay, P. J.; Wadt, W. R. *J. Chem. Phys.* **1985**, *82*, 270. Wadt, W. R.; Hay, P. J. *J. Chem. Phys.* **1985**, *82*, 284. Hay, P. J.; Wadt, W. R. *J. Chem. Phys.* **1985**, *82*, 299. The BLYP exchange-correlation functional is described in Becke, A. D. *Phys. Rev. A* **1988**, *38*, 3098. Lee, C.; Yang, W.; Parr, R. G. *Phys. Rev. B* **1988**, *37*, 785.
31. Peng, C.; Schlegel, H. B. *Isr. J. Chem.* **1993**, *33*, 449.
32. Lohrenz, J. C.; Woo, T. K.; Ziegler, T. *J. Am. Chem. Soc.* **1995**, 12973.